Molecular Biology of the Cell
Vol. 14, 2057–2070, May 2003

XBX-1 Encodes a Dynein Light Intermediate Chain Required for Retrograde Intraflagellar Transport and Cilia Assembly in *Caenorhabditis elegans* [V]

Jenny C. Schafer,*† Courtney J. Haycraft,*† James H. Thomas,‡ Bradley K. Yoder,*§ and Peter Swoboda¶§

*Department of Cell Biology, University of Alabama at Birmingham Medical Center, Birmingham, Alabama 35294; ‡Department of Genome Sciences, University of Washington, Seattle, Washington 98195; and ¶Karolinska Institute, Department of Biosciences, Södertörn University College, Section of Natural Sciences, S-14189 Huddinge, Sweden

Submitted October 22, 2002; Revised December 13, 2002; Accepted December 27, 2002
Monitoring Editor: Mary Beckerle

Intraflagellar transport (IFT) is a process required for flagella and cilia assembly that describes the dynein and kinesin mediated movement of particles along axonemes that consists of an A and a B complex, defects in which disrupt retrograde and anterograde transport, respectively. Herein, we describe a novel *Caenorhabditis elegans* gene, *xbx-1,* that is required for retrograde IFT and shares homology with a mammalian dynein light intermediate chain (D2LIC). *xbx-1* expression in ciliated sensory neurons is regulated by the transcription factor DAF-19, as demonstrated previously for genes encoding IFT complex B proteins. XBX-1 localizes to the base of the cilia and undergoes anterograde and retrograde movement along the axoneme. Disruption of *xbx-1* results in cilia defects and causes behavioral abnormalities observed in other cilia mutants. Analysis of cilia in *xbx-1* mutants reveals that they are shortened and have a bulb like structure in which IFT proteins accumulate. The role of XBX-1 in IFT was further confirmed by analyzing the effect that other IFT mutations have on XBX-1 localization and movement. In contrast to other IFT proteins, retrograde XBX-1 movement was detected in complex A mutants. Our results suggest that the DLIC protein XBX-1 functions together with the CHE-3 dynein in retrograde IFT, downstream of the complex A proteins.

INTRODUCTION

Transport mechanisms that utilize microtubule based kinesin and dynein motor proteins play a variety of important functions in cells such as movement of vesicles and organelles, chromosomal segregation, Golgi organization, and intraflagellar transport (IFT; Mitchell, 1994; Porter, 1996; Vaisberg *et al.*, 1996; Hirokawa, 1998; Pazour *et al.*, 1999; Porter *et al.*, 1999; Signor *et al.*, 1999a; Goldstein, 2001). IFT is required for flagella and cilia assembly that describes the anterograde and retrograde migration of protein particles from the base to the tip of the cilia and back to the base, respectively (Signor *et al.*, 1999a; Rosenbaum, 2002).

IFT appears to be a highly conserved process common to all ciliated eukaryotic organisms (Kozminski *et al.*, 1993; Signor *et al.*, 1999a; Haycraft *et al.*, 2001; Rosenbaum, 2002). Through biochemical approaches in *Chlamydomonas*, many of the IFT proteins have been assigned to one of several substructures in the IFT particle including the kinesin-II complex, complex A, complex B, and the dynein motor complex (Cole *et al.*, 1998; Pazour *et al.*, 1999; Porter *et al.*, 1999; Iomini *et al.*, 2001). In *Caenorhabditis elegans*, mutations that disrupt proteins in the kinesin or complex B result in severely stunted cilia (Perkins *et al.*, 1986; Collet *et al.*, 1998; Haycraft *et al.*, 2001). In contrast, mutations in complex A proteins or the dynein CHE-3 result in slightly shortened cilia axonemes with an accumulation of electron dense material along the axoneme compared with wild type (Perkins *et al.*, 1986; Signor *et al.*, 1999a). These data suggest that the kinesin-II and complex B proteins are required for the anterograde directed particle movement, whereas the complex A proteins and the dy-

Article published online ahead of print. Mol. Biol. Cell 10.1091/mbc.E02–10–0677. Article and publication date are at www.molbiolcell.org/cgi/doi/10.1091/mbc.E02–10–0677.

[V] Online version of this article contains video materials. Online version is available at www.molbiolcell.org.

§ Corresponding authors. E-mail addresses: Byoder@uab.edu; peter.swoboda@biosci.ki.se.

† Both authors contributed equally to this work.

nein function in retrograde transport (Cole *et al.*, 1998; Piperno *et al.*, 1998; Signor *et al.*, 1999a).

Dyneins are high-molecular-weight motor protein complexes that generate minus end directed movement along microtubules. There are two classes of dyneins: axonemal dyneins that are involved in cilia and flagella beating and cytoplasmic dyneins that are involved in IFT and intracellular trafficking (reviewed in Holzbaur and Vallee, 1994; Gibbons, 1995; Porter, 1996). Most dynein complexes consist of two heavy chains, two or more intermediate chains, several light intermediate chains, and numerous light chains. The heavy chains function as the ATPase and motor component, whereas the other accessory chains are thought to provide diversity through interactions with specific cargo molecules (Holzbaur and Vallee, 1994; Tynan *et al.*, 2000b; Karcher *et al.*, 2002).

Although the full composition of the dynein complex involved in IFT has yet to be determined, the dynein heavy chains have been identified in *Chlamydomonas* and *C. elegans* (Pazour *et al.*, 1999; Porter *et al.*, 1999; Signor *et al.*, 1999a; Wicks *et al.*, 2000). In *Chlamydomonas*, mutation of the dynein heavy chain (DHC1B) results in shortened flagella that exhibit IFT particle accumulation at the distal tips indicative of defective retrograde transport (Pazour *et al.*, 1999; Porter *et al.*, 1999). Similar results have been observed in *C. elegans* due to disruption of the dynein heavy chain CHE-3 (Perkins *et al.*, 1986; Signor *et al.*, 1999a; Wicks *et al.*, 2000).

Herein, we describe a novel gene in *C. elegans*, *xbx-1*, that shares significant similarity with the recently identified mammalian dynein light intermediate chain (D2LIC; Grissom *et al.*, 2002) as well as with a *Chlamydomonas* ortholog that functions in IFT (Perrone *et al.*, 2003). Expression of *xbx-1* is regulated by the DAF-19 transcription factor. The cilia of *xbx-1(ok279)* mutant worms are shortened and terminate in a bulb-like structure at the distal tip where IFT proteins accumulate. As is typical of proteins involved in IFT (Signor *et al.*, 1999a; Haycraft *et al.*, 2001; Qin *et al.*, 2001), XBX-1::YFP localizes to the base of cilia and migrates along the axoneme in both anterograde and retrograde directions. In contrast to results obtained with other IFT proteins, retrograde movement of XBX-1::YFP was normal in complex A mutants. Together, these data suggest that the light intermediate chain subunit of the dynein complex, XBX-1, functions as part of the retrograde motor for IFT.

MATERIALS AND METHODS

General Molecular Biology Methods

General molecular biology procedures were performed according to standard protocols (Sambrook *et al.*, 1989). Cloned worm DNA, total worm DNA, worm cDNA, or single worms were used for PCR amplifications, for direct sequencing, or for subcloning (Sambrook *et al.*, 1989). Clones, primer sequences, and PCR conditions are available on request. DNA sequencing was performed either by MWG Biotech (http://www.mwg-biotech.com/html/index.shtml; Ebersberg, Germany) or the UAB Genomics Core Facility of the Heflin Center for Human Genetics.

DNA Sequence Analyses

Genome sequence information used in this study was obtained from the National Center for Biotechnology Information (http://www.ncbi.nlm.nih.gov/), from the *C. elegans* Genome Sequencing Centers (http://www.sanger.ac.uk/Projects/C_elegans/; http://genome.wustl.edu/projects/celegans/; Consortium, 1998) or from the Celera Database (http://www.celera.com/). Gene identities were derived from the *C. elegans* database WormBase or references therein (http://www.wormbase.org/; Stein *et al.*, 2001). BLAST and visual inspection were used to identify and evaluate orthologues of XBX-1 (http://www.ncbi.nlm.nih.gov/BLAST/; Altschul *et al.*, 1997).

The *C. elegans* genome sequence wide search for putative transcriptional target genes of the RFX-type transcription factor DAF-19 was conducted using a specially designed computer search algorithm (K. Bubb and P. Swoboda, unpublished information), which searches for the X-box promoter element consensus sequence (Swoboda *et al.*, 2000; Haycraft *et al.*, 2001) upstream of the translational start site (ATG) of genes or predicted genes. *F02D8.3* was one in a list of candidate genes that fit the experimental criteria and, when mutated, resulted in phenotypes that had previously been described for direct transcriptional DAF-19 targets (Swoboda *et al.*, 2000; Haycraft *et al.*, 2001). Thus, the gene *F02D8.3* was renamed *xbx-1* for *X-box* promoter element regulated gene.

Strains

General growth conditions for *C. elegans* strains were as described (Brenner, 1974). Strains were grown at 20°C unless stated otherwise. The wild-type strain was N2 Bristol. The following mutations were used: LG (linkage group) I: *che-3*(*e1124*), *che-13(e1805)*; LG II: *daf-19*(*m86*), *dpy-10(e128), unc-52(e444)*; LG III: *dpy-1*(*e1*), *unc-32*(*e189*); LG IV: *daf-10(e1387), dpy-20(e1282), him-8*(*e1489*), *unc-24*(*e138*); LG V: *che-11(e1810), dyf-4*(*m158*), *dpy-11*(*e224), osm-6(p811), unc-76*(*e911*), *xbx-1*(*ok279*); LG X: *lin-15(n765), osm-5(m184).* The following extrachromosomal arrays were used: *saEx523, yhEx105, yhEx107, and yhEx109* were used for *xbx-1::gfp* expression experiments; *yhEx19* was used for OSM-5::GFP localization analyses (Haycraft *et al.*, 2001); *yhEx80* was used for OSM-6::YFP localization studies; *yhEx100* was used for XBX-1::YFP localization studies; *myEx10* was used for CHE-11::GFP localization studies (Qin *et al.*, 2001). All strains used and strain construction details are available on request.

Isolation, Genetic, and Molecular Characterization of the Deletion Allele xbx-1(ok279) V

The deletion allele *ok279* was generated by the *C. elegans* Gene Knockout Consortium (http://elegans.bcgsc.bc.ca/knockout.shtml) using publicly available methodology (http://www.mutantfactory-.ouhsc.edu/protocols.asp; Anderson, 1995). The original mutated strain carrying the deletion allele *ok279* was out-crossed seven times with N2 and CB2065: *dpy-11* (*e224*) *unc-76* (*e911*) V, eventually resulting in the homozygous mutant strain JT11069: *xbx-1* (*ok279*) V, which was then used as the basis for all further analyses. Using standard genetic crossing methods and fluorescent dye filling assays we determined 1) that *xbx-1*(*ok279*) V is fully recessive and 2) that *xbx-1*(*ok279*) V complements another gene, *dyf-4*(*m158*) V, that maps nearby and results in a Dyf phenotype (Starich *et al.*, 1995). In fluorescent dye filling assays the progeny of *dyf-4(m158)* heterozygous males crossed to *xbx-1(ok279)* homozygous hermaphrodites behaved similarly to wild-type and other control cross progeny (our unpublished results). Thus, *xbx-1* and *dyf-4* are different genes. After restriction enzyme mapping the deletion allele *ok279* was DNA sequenced directly from purified bulk PCR products that spanned the deletion from both sides. The *ok279* deletion extends over 1610 base pairs starting in the intron between exons 3 and 4 and ending 30 base pairs after the STOP codon (cosmid F02D8 base pairs 25954–27563 are deleted; Figure 1D).

Assays

Fluorescent dye-filling assays were performed as described (Malone and Thomas, 1994; Starich *et al.*, 1995; Fujiwara *et al.*, 1999) using FITC (Sigma, St. Louis, MO), DiI-C12 or DiD (Molecular Probes, Inc., Eugene, OR). Adult hermaphrodites were observed at 1000×

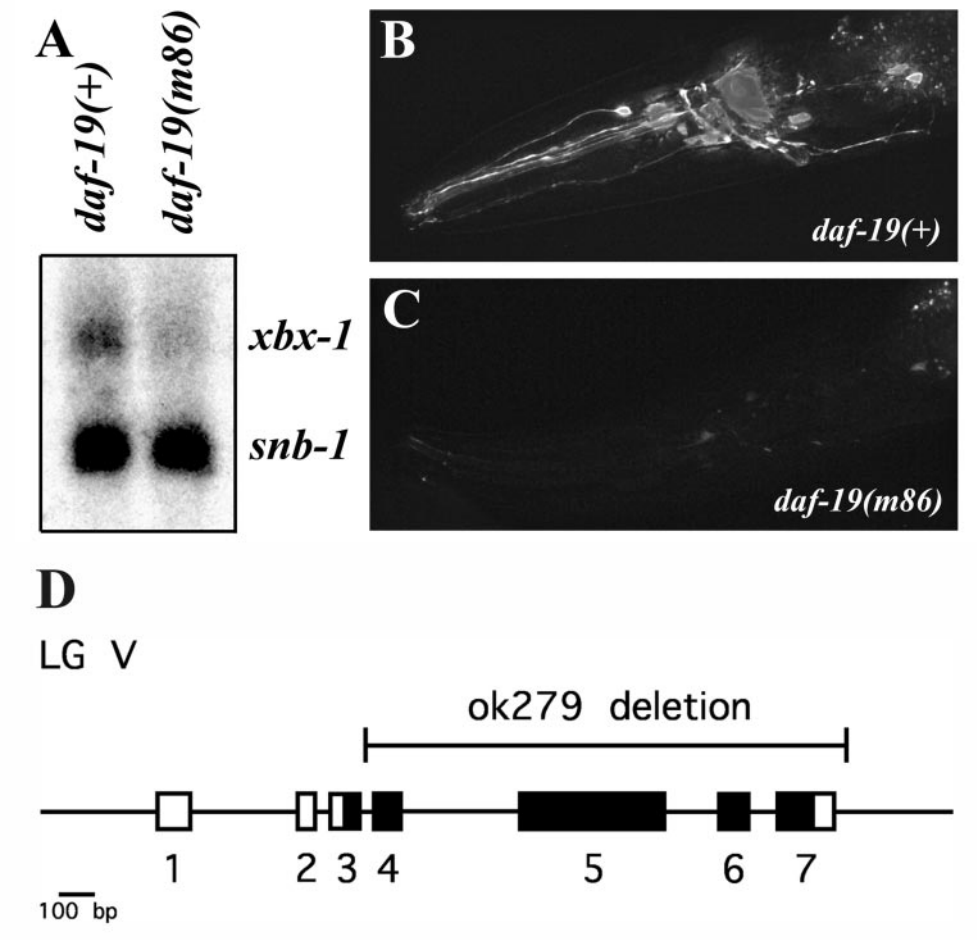

Figure 1. DAF-19 regulation of *xbx-1* expression. (A) Northern blot analysis of *xbx-1* expression in *daf-19*(+) and *daf-19*(*m86*) worms. *xbx-1* expression is reduced in *daf-19*(*m86*) worms. The DAF-19 independent gene *snb-1* was used as a loading control. (B and C) In vivo analysis of *xbx-1* promoter driven GFP expression in (B) *daf-19*(+) and (C) *daf-19*(*m86*) mutant worms. *xbx-1* is expressed in the ciliated sensory neurons of the wild-type worms. *xbx-1* expression is significantly reduced in the absence of DAF-19. Anterior of the worm is directed toward the left. (D) Genomic organization of the *xbx-1* gene (*F02D8.3*), which maps on linkage group (LG) V. Numbered boxes, exons; black boxes, exons with significant sequence similarities to DLIC proteins from other species (cf. Grissom *et al.*, 2002, and Perrone *et al.*, 2003). The region of the gene deleted in the *xbx-1(ok279)* mutant allele is shown above the schematic.

magnification by conventional fluorescence microscopy (Zeiss Axioplan 2, Carl Zeiss MicroImaging, Thornwood, NY) and at the highest magnification on a standard stereo dissecting microscope (Olympus Optical SZX12, Oympus America, Melville, NY) equipped with a fluorescent light attachment.

Osmotic avoidance assays were performed essentially as described (Culotti and Russell, 1978) by testing whether adult hermaphrodites placed in the center of a ring of high osmotic strength (8 M glycerol) will cross that ring or not during a time period of 10 min.

A semiquantitative assessment of male mating efficiency was made as described by Starich *et al.* (1995) with slight modification. Five L4 or young adult males were placed on a regular agar plate together with two L4 hermaphrodites, respectively. Hermaphrodites were one of the following two genotypes: 1) JT7273: *unc-24*(*e138*) *dpy-20*(*e1282*) IV; or 2) SP17: *unc-32*(*e189*) *dpy-1*(*e1*) III. For the mutations *che-13* I, *dyf-4* V and *xbx-1* V, double mutants were constructed using *him-8* IV, which then segregated homozygous mutant male progeny for mating tests. Numbers of cross-progeny were counted for each cross and compared with appropriate controls involving N2 or *him-8* males. At least four separate crosses using two different types of marked hermaphrodites were performed for each mutant tested.

Generation and Analyses of the xbx-1::gfp Expression Constructs

A genomic fragment consisting of 2 kb of the promoter region upstream of *xbx-1* was amplified from cloned worm DNA by PCR. The primers contained restriction enzyme sites for ligation into the GFP vector pPD95.77 (gift of A. Fire). The promoter, containing the wild-type X-box element, was fused in-frame to the GFP gene at codon ten of *xbx-1*. This fusion was introduced into worms by germline transformation at 100 ng/μl by using standard methods (Mello *et al.*, 1991) using *lin-15*(+) at 60 ng/μl as a cotransformation marker DNA (Huang *et al.*, 1994), and expression levels were analyzed as previously described (Swoboda *et al.*, 2000; Haycraft *et al.*, 2001).

Generation of Constructs and Strains Used for Localization Studies

For *xbx-1* rescue experiments and analysis of XBX-1::YFP localization, a general YFP expression vector was derived from pPD95.81 vector (gift of A. Fire) by replacing GFP with YFP from pPD132.102 (gift of A. Fire) using the restriction enzymes *NcoI* and *MfeI*. The 250-base pair *osm-5* promoter was cloned into this vector (Haycraft *et al.*, 2001) along with the 2.2-kb *xbx-1* or 3.1-kb *osm-6* (Collet *et al.*, 1998) coding region from N2 genomic DNA to create the *osm-5::xbx-1::yfp* or *osm-5::osm-6::yfp* expression vector, respectively. Genomic DNA for cloning was amplified using AccuTaq LA Polymerase Mix (Sigma-Aldrich, St. Louis, MO). Germline transformations were carried out as previously described (Mello *et al.*, 1991). Wild-type or *xbx-1(ok279)* adult hermaphrodites were injected with 1–5 ng/μl test DNA and pRF4, which contains the dominant marker *rol-6(su1006)* (Mello *et al.*, 1991). Transgenic worms were identified

Table 1. X-box sequence in the promoter region of *xbx-1* and its putative orthologs

Species	Location[a]	X-box Sequence[b]
C. elegans	−79 to −66 ATG	**G T** T T **C C** AT **G G T A A C**
C. briggsae	−93 to −80 ATG	**G T** T T **C C** AT **G G T** T **A C**
Drosophila	−68 to −54 ATG	**G T** T **G C** T AGT **A G C A A C**
Human	−67 to −54 ATG	**G** C T C **C C** AT **G G C A A C**
Consensus X-box		**G T N R C C N (0–3) R G Y A A C**

[a] ATG denotes translational start site.

[b] R = G/A; Y = C/T; N = G/A/T/C; bold denotes a match to the mammalian X-box consensus sequence (Emery *et al.,* 1996).

Note: The sequence of the five prime end of the mouse ortholog has not yet been completed and thus the presence of an X-box could not be evaluated.

based on the right-handed roller phenotype (Rol) and maintained by picking Rol hermaphrodites.

To obtain transgenic mutant strains used for localization and cilia morphology analyses, adult Rol males carrying the desired extrachromosomal array were mated to homozygous mutant hermaphrodites. F_1 hermaphrodites were screened for the Rol phenotype and allowed to self-fertilize. F_2 hermaphrodites were screened for the presence of Rol and subsequently screened by fluorescent dye-filling to identify homozygous mutant hermaphrodites.

Imaging

For imaging, adult worms were anesthetized in 10 mM levamisole and mounted on 2% agar. Time-lapse imaging of worms expressing *xbx-1::yfp* was performed on an Olympus IX70 inverted microscope and captured with a Retiga 1300 cooled CCD camera (Qimaging, Burnaby, BC, Canada). Shutters and filters were computer driven. Images were acquired for at least 15 s at ~2 frames/s using IPLab Spectrum 3.6 (Scanalytics, Fairfax, VA). Movies were then exported into Quicktime (Adobe Systems, Inc., San Jose, CA) and sequential still frames were taken from Quicktime movies. Localization and morphology images were captured using a Leica Confocal Imaging Spectrophotometer TCS SP unit mounted on a Leica DMIRBE inverted research microscope (Leica Microsystems, Bannockburn, IL). Further processing of images was done using Photoshop 6.0 and AfterEffects 6.0 (Adobe Systems, Inc., San Jose, CA). QuickTime (Adobe Systems, Inc.) movies were created at a rate of two frames per second.

Northern Blot Analysis

RNA for Northern blot analysis was isolated from mixed stage worms by addition of 5 volumes 5 M guanidine isothiocyanate followed by homogenization using a PowerGen 700 (Fisher Scientific, Pittsburgh, PA), centrifugation at 6000 × *g* to remove particulate matter, and purification over a CsCl cushion. Total RNA was purified over oligo-dT cellulose (Stratagene, La Jolla, CA) to obtain poly-A–enriched RNA. Radiolabeled *xbx-1* and *snb-1* (Nonet *et al.*, 1998) probes were created using the Random Prime-A-Gene kit (Promega, Madison, WI) according to the manufacturer's instructions. Strains used for Northern analyses contained *daf-12(sa204) X*, which suppresses the Daf-c phenotype of *daf-19(m86)* worms.

RESULTS

Transcriptional Regulation of xbx-1

Several genes involved in IFT and ciliogenesis in *C. elegans* have been identified (Cole *et al.*, 1998; Collet *et al.*, 1998; Signor *et al.*, 1999b; Wicks *et al.*, 2000; Haycraft *et al.*, 2001; Qin *et al.*, 2001). In the case of the IFT complex B genes, all are regulated by the DAF-19 transcription factor (Swoboda *et al.*, 2000; Haycraft *et al.*, 2001). This regulation occurs through an X-box promoter element generally located within the first 150 nucleotides upstream of the translational start site (ATG). In a previous genome sequence–based search, the gene *xbx-1* (*F02D8.3*) was identified as a candidate DAF-19 target because of the presence of an X-box sequence located at position −79 upstream of the predicted ATG (Swoboda *et al.*, 2000).

XBX-1 shares homology with a recently identified mammalian dynein light intermediate chain (DLIC) known as D2LIC (Grissom *et al.*, 2002). Putative orthologs are also present in *Chlamydomonas*, *Drosophila,* and *Caenorhabditis briggsae* (Perrone *et al.*, 2003, and our unpublished results). Interestingly, a near consensus X-box sequence was also detected in the promoter region of the putative *xbx-1* orthologs in human, *C. briggsae*, and *Drosophila* (Table 1). These data suggest that *xbx-1* and its orthologs in higher eukaryotes are regulated though a common transcriptional mechanism. Intriguingly, cross-species comparisons have also identified similar promoter regions in genes encoding several other IFT complex B proteins (B.K. Yoder and P. Swoboda, unpublished results).

To determine whether *xbx-1* is regulated by DAF-19, we compared the level of *xbx-1* expression in wild-type and *daf-19* mutant worms. By Northern blot analysis, we determined that the expression of *xbx-1* was nearly abolished in the absence of DAF-19 (Figure 1A). To further establish the importance of DAF-19 in *xbx-1* expression, we measured GFP expression in wild-type (*daf-19(+)*) and *daf-19* mutant strains (*daf-19(m86)*) carrying the *xbx-1* promoter region fused to the GFP gene (see MATERIALS AND METHODS). In wild-type worms, *xbx-1::gfp* expression is detected in ciliated sensory neurons and like the results obtained on the Northern blot, mutation of *daf-19* caused a significant reduction in the level of *xbx-1::gfp* expression compared with wild-type N2 background (Figure 1, B and C, and Table 2).

Generation and Characterization of the xbx-1 Deletion Mutant

To begin analyzing the role of *xbx-1*, the *C. elegans* knockout consortium screened a mutant library for worm strains carrying a deletion in *xbx-1* (see MATERIALS AND METH-

Table 2. *xbx-1* expression analyses using an in vivo GFP expression assay

Genotype	Wild type			*daf-19(m86)*		
Strength of Expression	Strong	Weak	Absent	Strong	Weak	Absent
xbx-1::*gfp*						
line 1	86	14	0	1	37	62
line 2	66	31	3	1	33	66
line 3	61	33	6	0	22	78
line 4	51	41	8	0	3	97

Data are given as percent expression in ciliated sensory neurons in the head of adult animals. Only the ciliated sensory neurons adjacent to the nerve ring were examined. To classify expression as "strong," "weak," or "absent," the number of neurons expressing *xbx-1*::*gfp* as well as the visibility of GFP in neuronal cell bodies and in processes extending to the tip of the nose were taken into consideration. Four independent transgenic lines were analyzed. Each row represents the data for one transgenic line. For each transgenic line (containing the wild-type X-box promoter element sequence) the transgene was also moved from wild type into a *daf-19* mutant background. Eighty to 120 animals were analyzed for each transgenic line.

ODS). One allele, *xbx-1(ok279),* was identified that carried a 1610-base pair deletion starting in the middle of the third intron and ending 30 base pairs after the translational termination codon (base pairs 25,954–27,563 are deleted in the cosmid F02D8 sequence). The *ok279* deletion would truncate the 369 amino acid XBX-1 protein at position 87 and therefore most likely represents a functional null allele (Figure 1D).

Ciliary and Sensory Defects in xbx-1 Mutants

Because mutations in several other X-box containing and DAF-19 regulated genes have been shown to result in ciliary and sensory defects (Collet *et al.*, 1998; Swoboda *et al.*, 2000; Haycraft *et al.*, 2001), we analyzed *xbx-1* mutant worms for such phenotypes. A first approach often used to evaluate whether sensory cilia are correctly formed is the fluorescent dye-filling assay. In wild-type worms, some of the sensory neurons that extend cilia through the cuticle into the environment allow fluorescent dye uptake into these sensory neurons. As is seen in other IFT mutants (Perkins *et al.*, 1986; Collet *et al.*, 1998; Haycraft *et al.*, 2001), *xbx-1(ok279)* worms failed to absorb fluorescent dye (Dyf phenotype; Figure 2B and Table 3), suggesting that cilia are either malformed in *xbx-1(ok279)* worms or that the cilia do not extend through the cuticle.

Defects in the cilia of the sensory neurons in *C. elegans* are associated with characteristic changes in behavior, including the inability to avoid substances of high osmotic strength (Osm phenotype), defects in chemotaxis (Che phenotype) toward attractants as well as a reduction in mating efficiency (Starich *et al.*, 1995). To determine if the deletion of *xbx-1* resulted in behavioral defects similar to that seen for other ciliogenic mutants, we conducted an osmotic avoidance assay. In this assay, we measured the frequency with which *xbx-1(ok279)* worms crossed a ring of 8 M glycerol on agar plates. Wild-type control N2 worms were found to cross the osmotic barrier at a rate of <5%. In contrast, worms lacking *xbx-1* were found to cross the barrier at a rate >80%, a result similar to that seen for other mutants lacking sensory ciliary function such as *che-13(e1805)* and *dyf-4(m158)* (Table 3; Starich *et al.*, 1995).

To further confirm the ciliary defects, we analyzed male *xbx-1*(*ok279*) worms for their mating efficiency. Male mating behavior, in particular the ability to locate the hermaphrodite vulva is mediated through cilia that extend off sensory neurons located in specialized rays in the male tail (Liu and Sternberg, 1995). Loss of cilia function has been shown to cause a significant reduction in mating efficiency (Starich *et al.*, 1995). Our analysis of *xbx-1* mutants revealed a mating efficiency significantly <30% as efficient as wild type (Table 3). For comparison, *che-13*(*e1805*) has a mating efficiency of 0%, and both *dyf-4*(*m158*) and wild-type N2 have mating efficiencies of 100%. The defects in *xbx-1(ok279)* mating efficiency are milder than in *che-13(e1805),* but more severe than in *dyf-4*(*m158*). Thus, *xbx-1* mutants have a measurable sensory defect with regard to male mating.

Transgenic Rescue of xbx-1(ok279) Ciliary Defects

To confirm that the *ok279* deletion is responsible for the defects in *xbx-1* mutants, we constructed *xbx-1* mutant lines that express the wild-type *xbx-1* gene fused to the yellow fluorescent protein (YFP) as a transgene. Expression in these transgenic strains was under control of the DAF-19 regulated *osm-5* promoter (Haycraft *et al.*, 2001), which, like the *xbx-1* promoter, drives expression in many ciliated sensory neurons. The effect on the cilia phenotype was evaluated using the fluorescent dye-filling assay. As indicated previously, *xbx-1* mutants were not able to absorb dye (Figure 2B), however, all of the rescued lines tested (n = 4) were able to absorb dye, indicating the restoration of normal cilia (Figure 2, A and C). These data verify that the *ok279* deletion is responsible for the *xbx-1* phenotype.

Localization and Movement of XBX-1 Protein within Cilia

To analyze the possible role of XBX-1 in the IFT process, we utilized transgenic worm strains expressing XBX-1 protein tagged with YFP to evaluate XBX-1 localization and movement within sensory neurons. The XBX-1::YFP protein was detected specifically at the transition zone at the base of the cilia and in the axoneme (Figure 2C), consistent with a role

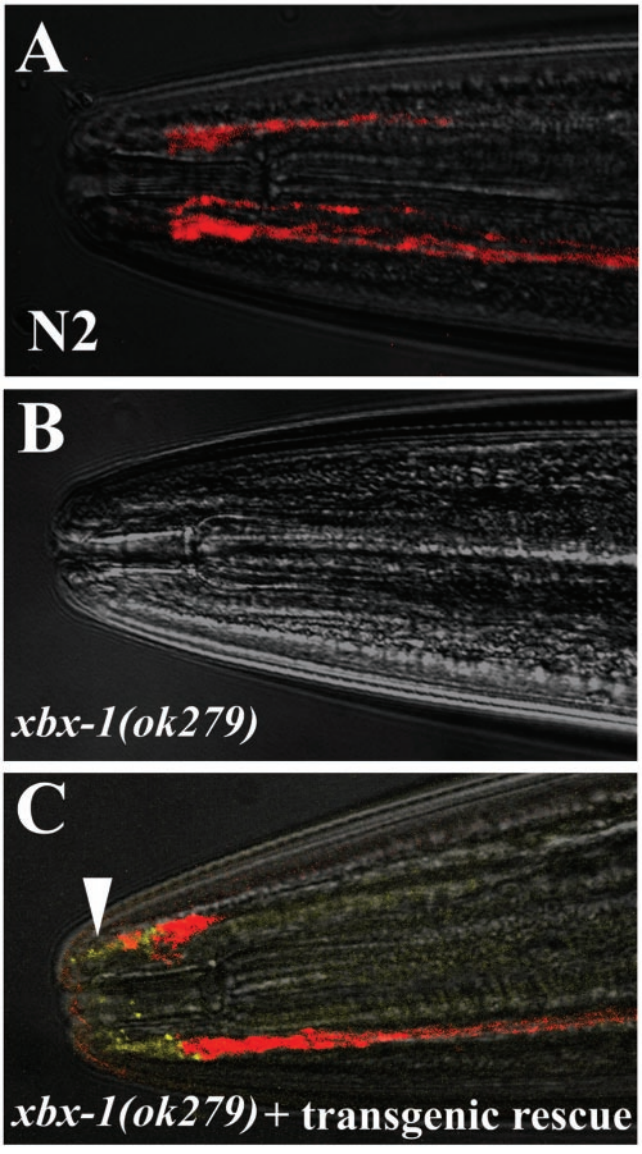

Figure 2. Restoration of cilia in *xbx-1* mutants by transgenic rescue. All panels are bright field images overlaid with fluorescent images to show dye-filling (red) and XBX-1:: YFP localization (yellow). (A) Six pairs of amphid neurons of wild-type N2 worms fill with the fluorescent dye DiD. (B) In contrast, *xbx-1(ok279)* mutant worms fail to take up the dye. (C) Transgenic expression of *xbx-1::yfp* in *xbx-1(ok279)* mutant worms restores the ability to uptake fluorescent dye (red). The XBX-1::YFP protein is detected at the transition zones and within cilia on the ends of the amphid neurons (yellow, arrowhead). Anterior is toward the left in all panels.

in IFT. Furthermore, using time-lapse fluorescence microscopy, XBX-1::YFP particles were detected migrating along the cilium axoneme in both anterograde and retrograde directions similar to known IFT proteins (Figure 3; Signor *et al.*, 1999a; Haycraft *et al.*, 2001; Qin *et al.*, 2001). These results, along with the ciliary defects observed in *xbx-1* mutants, demonstrate a role for XBX-1 in the IFT process.

Table 3. Analysis of *xbx-1(ok279)* mutant phenotypes

Genotype	Fluorescent dye-filling[a]	Osmotic avoidance[b]	Male mating efficiency (%)[c]
N2 (wild type)	+	+	100
che-13(e1805)	−	−	0
dyf-4(m158)	−	−	≥100
xbx-1(ok279)	−	−	8

[a] Using the fluorescent dyes FITC and DiI-C12, 100% of wild-type animals exhibited staining of 6 amphid neurons (occasionally an animal stained only 4 or 5) and 2 phasmid neurons, whereas all three mutant strains tested did not exhibit any staining, either in amphid or in phasmid neurons. At least 3 separate experiments were performed using a total of >50 adult hermaphrodites per strain.

[b] Less than 5% of wild-type animals and >80% of all three mutant strains tested crossed a ring of high osmotic strength (8 M glycerol) during a time period of 10 min. At least 4 separate experiments were performed using a total of 55 to 90 adult hermaphrodites per strain.

[c] Data are given as percent mating efficiency (ME) compared with N2 wild type (set to 100%). Combined data from two independent, representative crosses are shown. Percentages as shown translate to the standard *C. elegans* ME scale (cf. Starich *et al.*, 1995) as follows: ME = 4 (30–100% as efficient mating as N2 wild type), ME = 3 (10–30% as efficient), ME = 2 (1–10% as efficient), ME = 1 (<1% as efficient), ME = 0 (no detectable mating). In repeated crosses *xbx-1* mutant males displayed an ME = 2–3.

xbx-1 Mutants Display Specific Ciliary Defects

There is a large collection of mutations that disrupt cilia formation in *C. elegans*, some of which impinge directly on the IFT process. The ciliary phenotype in many of these IFT mutants has been extensively analyzed by morphological description at the level of serial section transmission electron microscopy. Interestingly, the differences in the cilia morphology observed in the IFT mutants correlate nicely with whether the mutation disrupts a protein that functions as part of complex A, complex B, or the dynein motor complex. For example, in *osm-1*, *osm-5*, *osm-6*, and *che-13* mutants, the cilia are severely stunted and have ectopic posteriorly directed cilia-like projections (Perkins *et al.*, 1986). The analysis of the corresponding proteins affected in these mutants revealed that they are all orthologs of IFT complex B proteins identified biochemically in *Chlamydomonas* (Cole *et al.*, 1998; Qin *et al.*, 2001). The cilia phenotype exhibited by complex B mutants is supportive of their function in anterograde transport because the IFT particles fail to enter and migrate from the base to the distal tip of the cilia but rather accumulate at the transition zones. In the *daf-10* and *che-11* complex A mutants, cilia were slightly stunted relative to wild type, and contained dense material interspersed throughout swollen axonemes (Perkins *et al.*, 1986; Qin *et al.*, 2001). In the *che-3* dynein heavy chain mutant, the cilia axoneme is shorter than that of the complex A mutants with a similar accumulation of dense material in the swollen tip (Perkins *et al.*, 1986; Signor *et al.*, 1999a). In both the *che-3* and complex A mutant worms as well as in complex A mutants in *Chlamydomonas* the phenotype has been attributed to defects in retrograde transport (Piperno *et al.*, 1998; Pazour *et al.*, 1999; Porter *et al.*, 1999; Signor *et al.*, 1999a).

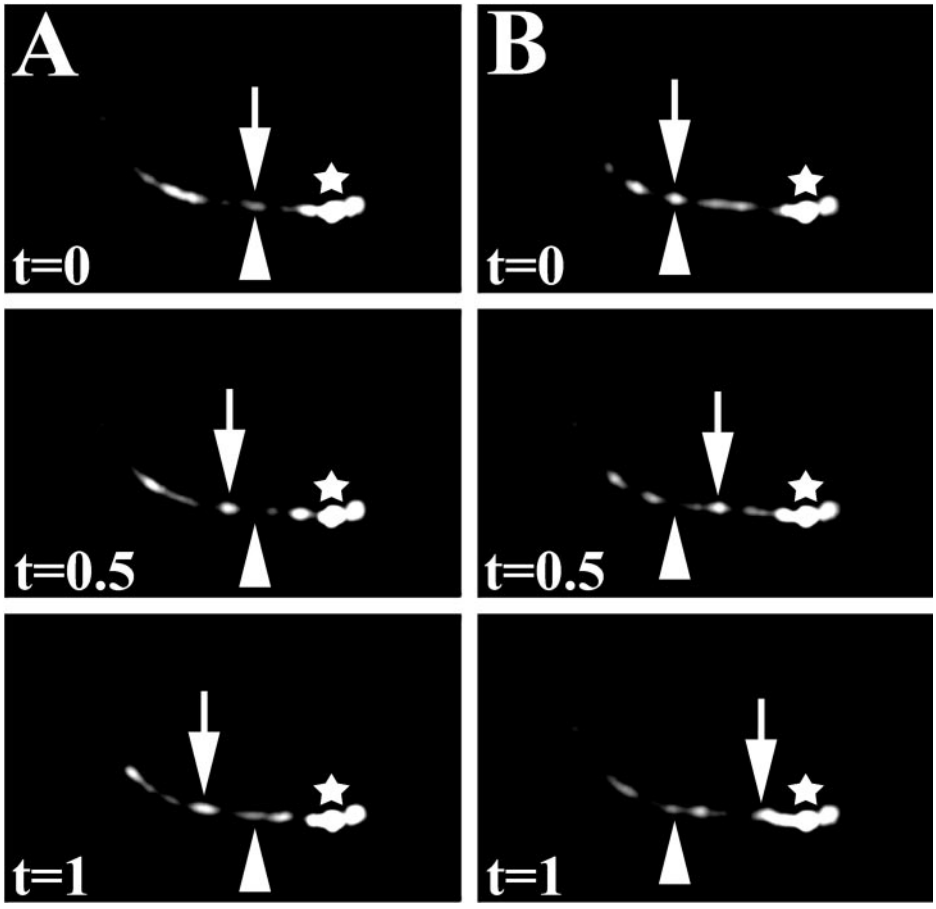

Figure 3. Movement of XBX-1::YFP along the cilia axoneme in phasmid neurons of a wild-type hermaphrodite. Using time-lapse fluorescence image analysis, XBX-1::YFP movement was observed in both (A) anterograde and (B) retrograde directions similar to that seen for other IFT proteins (Signor *et al.*, 1999a; Haycraft *et al.*, 2001; Qin *et al.*, 2001). The transition zone is marked (*). The arrowhead indicates the initial position of the particle at time zero ($t = 0$). The arrows indicate the same particle at subsequent times ($t = 0.5$ s, and $t = 1$ s). The distal tips of the phasmid cilia are directed toward the left. Three sequential frames from Movie 1 are shown for each.

The correlation between the cilia morphology and the function of the protein affected by the mutation suggests that we may be able to glean insight into the role of XBX-1 by comparing its ciliary phenotype to that seen in other known mutants that affect complex A, complex B, or the CHE-3 dynein. To conduct this analysis, we used fluorescence-tagged OSM-5 or OSM-6 (complex B) proteins to visualize the cilia morphology in wild-type, *xbx-1(ok279)*, *che-11(e1810)* (complex A mutant), *osm-5(m184)* (complex B mutant), and *che-3(e1124)* (dynein heavy chain mutant) worms. In wild-type worms, OSM-5::GFP localizes to the base of cilia and within cilia (Figure 4A). OSM-6::YFP shows an identical localization in wild-type worms (Collet *et al.*, 1998; Signor *et al.*, 1999a; and our unpublished results). Similar to the analysis described at the electron microscopy level, we could clearly distinguish between cilia morphology in mutants affecting complex B relative to that in complex A or the CHE-3 dynein using this G/YFP fusion protein approach (Figure 4). However, it was difficult to distinguish between the cilia morphology seen in complex A and the *che-3* mutants that both affect retrograde transport (Figure 4, C and D). Interestingly, our analysis of the *xbx-1(ok279)* worms indicated that the cilia morphology did not resemble those typified by complex B mutants. Rather, the cilia morphology in *xbx-1(ok279)* worms was indistinguishable from that seen in the complex A or *che-3* mutants (Figure 4, C–E). The cilia were stunted and contained massive accumulation of OSM-5::GFP in a bulb at the distal cilia tip. These results were surprising since there is an X-box sequence in the promoter of *xbx-1*. To date, X-box sequences have been identified in the promoter regions of complex B genes but not in the promoter regions of complex A genes or the IFT dynein (Swoboda *et al.*, 2000; Haycraft *et al.*, 2001). However, the ciliary phenotype of the *xbx-1* mutant supports a role for XBX-1 in retrograde IFT similar to that of the complex A proteins and CHE-3, but not in anterograde transport as proposed for the complex B proteins. Furthermore, the strong sequence similarity between XBX-1 and the DLIC protein D2LIC (Grissom *et al.*, 2002) is also suggestive of a role for XBX-1 in conjunction with CHE-3 in retrograde movement.

Effect of xbx-1 Mutation on the Localization of IFT Proteins

To evaluate what effect the loss of XBX-1 protein has on localization and movement of other proteins in the IFT particle, we moved extrachromosomal arrays that express known IFT proteins tagged with GFP or YFP into the *xbx-1* mutant background. Included in this analysis were two complex B proteins, OSM-5 and OSM-6, and a complex A protein, CHE-11. Because of the large size of *che-3* (~12 .4 kb

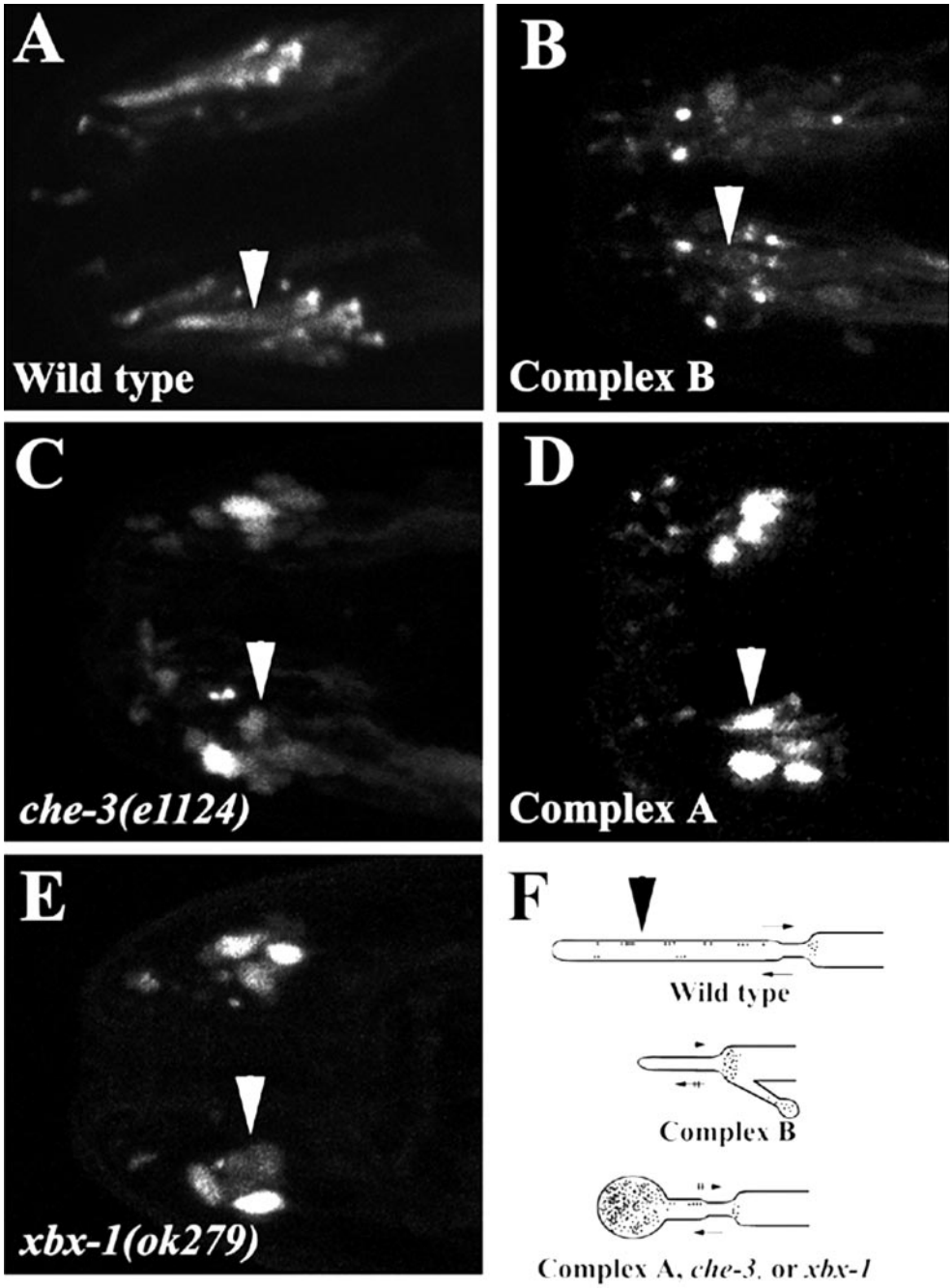

Figure 4. Analysis of cilia morphology in wild-type and IFT mutants using fluorescence-tagged IFT proteins. (A) OSM-5::GFP in wild-type worms shows full-length cilia with OSM-5::GFP localized at the transition zones and within cilia. (B) Complex B mutants (*osm-5* (*m184*)) exhibit severely truncated cilia axonemes as visualized by localization of OSM-6::YFP to the base of the truncated cilia. (C) Because of loss of retrograde IFT movement in *che-3* mutants, the cilia are severely shortened and exhibit a significant accumulation of OSM-5::GFP along the enlarged cilia axonemes. (D) The cilia in complex A mutants (*che-11(e1810)*) as determined by using OSM-5:: GFP are similar to those seen in the *che-3* mutants. The cilia are truncated and show significant accumulation of OSM-5::GFP along the swollen cilia axonemes. (E) Analysis of the cilia morphology in *xbx-1* mutants using OSM-5::GFP. Similar to that seen in both *che-3* and complex A mutants, the cilia of *xbx-1* mutants were truncated and OSM-5::GFP concentrated along the enlarged axonemes. (F) Schematic diagram depicting the cilia morphology as determined using the IFT::G/YFP fusion proteins. Arrows pointing right indicate retrograde movement while arrows pointing left indicate anterograde movement. Two lines drawn through the arrows indicate defects in transport. Images A–E are 2-D confocal projections from the amphid region of the worm. In all panels, arrowheads point to the cilia axonemes of one bundle of amphid neurons. The distal end of the cilium is directed toward the left in all panels.

transcript) we were unable to generate a GFP fusion protein to include in the analyses. As seen for OSM-5::GFP in *che-3* mutants (see Figure 4C), all the IFT proteins analyzed were found to accumulate in the bulb structure at the distal end of the cilia in *xbx-1* mutants, further supporting a role for XBX-1 in retrograde movement (Figure 5). Because all of the IFT proteins analyzed here enter the cilia efficiently, the data suggest that anterograde movement in the *xbx-1* mutants is not overtly affected and that XBX-1 function is not required for their assembly into the IFT particle at the base of cilia.

The Effect of Mutations in Other IFT Proteins on Localization of XBX-1::YFP

The IFT particle is a complex structure containing 17 or more proteins (Piperno and Mead, 1997; Cole *et al.*, 1998). The hierarchy with which these proteins assemble into the two complexes A and B and how these proteins interact to form the IFT particle is currently unknown. To determine where XBX-1 function is required during particle assembly or transport, we expressed XBX-1::YFP protein in the context of other ciliogenic

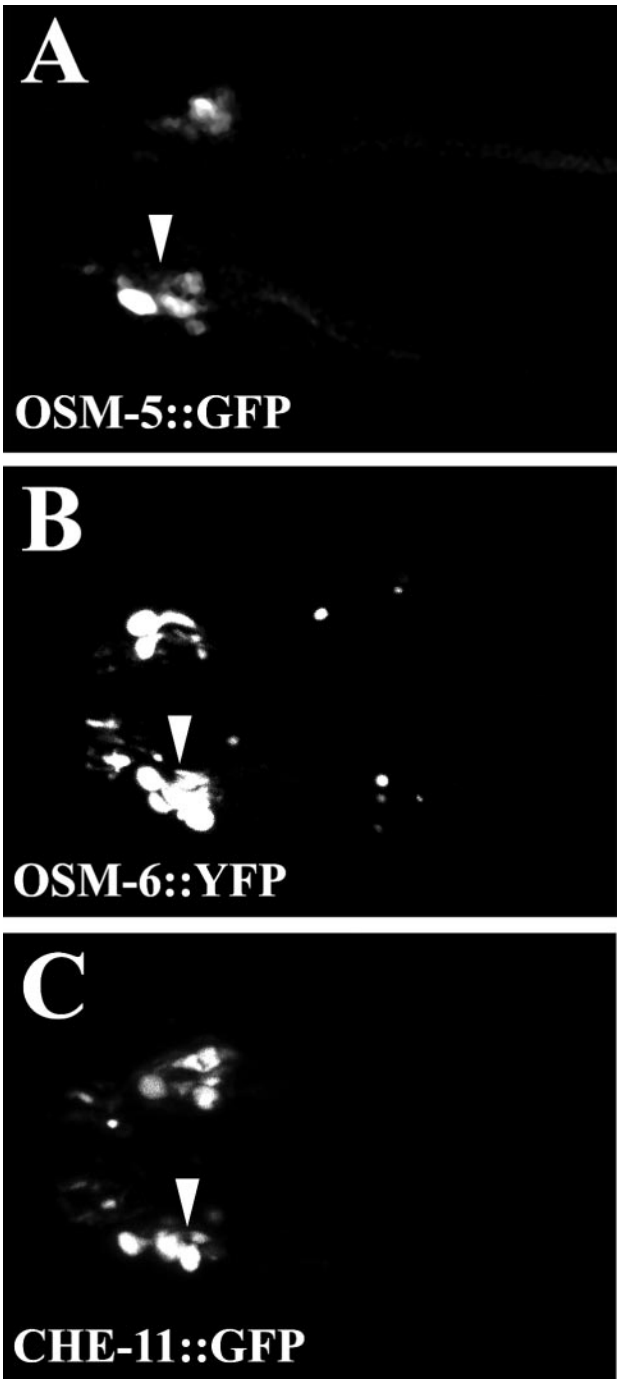

Figure 5. Localization of IFT proteins in *xbx-1* mutants. To evaluate the effect that the *xbx-1(ok279)* mutation has on the localization of IFT proteins, we crossed transgenic lines expressing either complex B or complex A IFT proteins fused to either GFP or YFP into the *xbx-1* mutant background. The loss of XBX-1 results in accumulation of both complex A and B proteins along the axoneme as shown using (A) OSM-5::GFP (complex B), (B) OSM-6::YFP (complex B), and (C) CHE-11::GFP (complex A). Arrowheads indicate the swollen cilia axonemes. Anterior of the worm and the distal tips of the cilia are directed toward the left. All panels are 2-D confocal projections.

mutant backgrounds that disrupt proteins in either complex B, complex A, or the dynein motor CHE-3. In complex B mutants such as *osm-5(m184),* XBX-1::YFP was retained at the base of the stunted cilia and in the severely stunted axonemes (Figure 6B), suggesting a defect in anterograde movement. Similarly, in complex A mutants, such as *che-11(e1810),* XBX-1::YFP was positioned at the cilia base and could also be detected in the shortened cilia axoneme extending off these transition zones (Figure 6C). These data suggest that the complex A and complex B proteins tested here are not critical for normal targeting or retention of XBX-1 to the transition zones at the base of the cilia. An interesting observation was that XBX-1::YFP does not accumulate in the axonemes of the complex A mutants (Figure 6C) as seen with IFT complex B proteins analyzed in complex A mutant backgrounds (Piperno *et al.*, 1998, and Figure 4D). These data suggest that retrograde transport of XBX-1 is still active in the absence of complex A. The transport of XBX-1 was further examined in the *che-3* mutants that lack a functional dynein that acts downstream of the complex A proteins during retrograde IFT. Unlike the result in the complex A mutants, our analysis of XBX-1::YFP in the *che-3(e1124)* strain revealed a significant accumulation of XBX-1::YFP in the massive bulb like structures at the distal tip of cilia as seen for all other IFT proteins analyzed in this mutant background (Figure 6D and our unpublished results).

Retrograde Movement of XBX-1::YFP in the Context of Complex A Mutants

The fact that XBX-1 does not accumulate in the cilia of complex A mutants raised the possibility that XBX-1 retrograde transport is not inhibited by loss of the complex A proteins. To test this possibility, we conducted time-lapse fluorescence imaging of XBX-1::YFP in *che-11* and *daf-10* complex A mutant backgrounds (Figure 7, and our unpublished results). Because of the low expression level of this fusion protein and the limiting sensitivity of the camera, it was difficult to obtain high-quality time-lapse images in these mutants. However, under visual inspection through the microscope, both anterograde and retrograde movement of XBX-1::YFP were clearly evident in the stunted cilia. This is further supported by the lack of accumulation of XBX-1 in the complex A mutants, which is distinct from complex A and complex B proteins analyzed in this background (Figure 4D and our unpublished results). Thus, retrograde transport of XBX1::YFP is still active in complex A mutants (Figure 7). Together with the accumulation of XBX-1::YFP in *che-3* mutants, these data support a role for XBX-1 and the CHE-3 dynein heavy chain in the retrograde transport of the IFT particle.

DISCUSSION

IFT was first observed in *Chlamydomonas* as a process required for flagella assembly (Kozminski *et al.*, 1993; Piperno and Mead, 1997). Subsequently, IFT has been reported in cilia assembly in *C. elegans* (Orozco *et al.*, 1999; Signor *et al.*, 1999a), and it is likely involved in flagella and cilia construction in higher eukaryotes as well (Pazour *et al.*, 2000, 2002; Yoder *et al.*, 2002). IFT is a process that describes the assembly of ciliary and flagellar proteins into large particles at the base of the organelle,

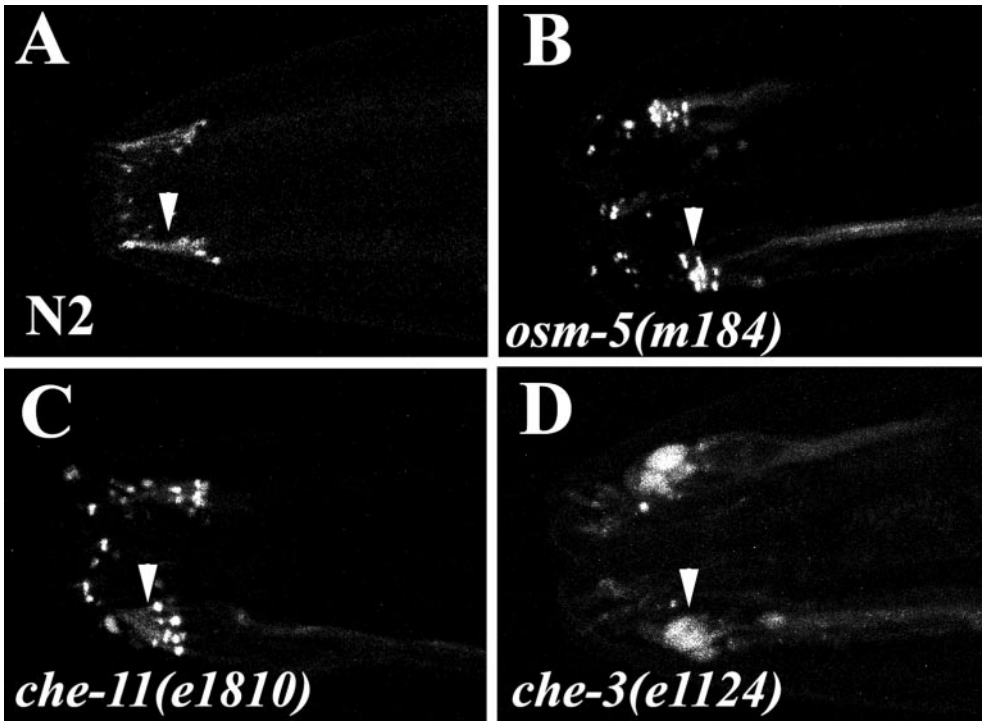

Figure 6. The effect of IFT mutations on XBX-1 localization. Localization of XBX-1::YFP was analyzed by moving the XBX-1::YFP transgene into the indicated IFT mutant backgrounds. (A) XBX-1::YFP localizes to the base of cilia and within cilia in wild-type N2 worms. (B) XBX-1::YFP localizes to the transition zone at the base of cilia in the *osm-5* complex B mutant, with little if any fluorescence detected along the cilia axoneme. (C) XBX-1::YFP is localized to the base of cilia in the *che-11* complex A mutant. Unlike other IFT proteins analyzed in complex A mutants, there is no significant accumulation of XBX-1::YFP within cilia (see Figure 4D). (D) XBX-1::YFP accumulates in large bulb-like endings in the *che-3* IFT dynein mutant. This is similar to that reported for other IFT proteins (see Figure 4C). Anterior of the worm and distal tip of the cilium are toward the left. Arrowheads indicate the position of the cilia axonemes on one bundle of amphid neurons.

transport of the particle toward the ciliary and flagellar tip through the action of the heterotrimeric kinesin-II complex, and return of the particle to the base utilizing a cytoplasmic dynein (Cole *et al.*, 1998; Piperno *et al.*, 1998; Orozco *et al.*, 1999; Signor *et al.*, 1999a, 1999b). Biochemical analysis of the IFT particle in *Chlamydomonas* indicates that the IFT particle consists of more than 17 peptides that form A and B complexes (Piperno and Mead, 1997; Cole *et al.*, 1998). How these complexes assemble, how they interact with one another in the IFT particle, and how they associate with the IFT motor proteins is still poorly understood.

Herein, we describe a novel gene, *xbx-1,* which shares strong sequence similarity with a DLIC protein recently identified in mammalian systems (Grissom *et al.*, 2002). Our analysis of *xbx-1* in *C. elegans* reveals that its function is required for IFT and cilia formation in sensory neurons. *xbx-1* was originally identified based on the presence of an X-box that is also present in the promoters of several ciliogenic genes encoding complex B IFT proteins (Swoboda *et al.*, 2000; Haycraft *et al.*, 2001). Our data confirm that *xbx-1* is regulated by DAF-19, that the XBX-1 protein localizes to the cilia base and moves along the axoneme typical of an IFT protein (Signor *et al.*, 1999a; Haycraft *et al.*, 2001; Qin *et al.*, 2001), and that disruption of *xbx-1* results in cilia defects causing sensory behavior defects common to other ciliogenic mutants (Starich *et al.*, 1995).

Surprisingly, despite the presence of an X-box sequence in the *xbx-1* promoter, the cilia morphology in *xbx-1* mutant worms did not resemble those typically seen in complex B mutants (Perkins *et al.*, 1986; Cole *et al.*, 1998; Haycraft *et al.*, 2001). Rather, the morphology is similar to that seen in mutants affecting retrograde transport such as complex A mutants or the CHE-3 IFT dynein mutant (Perkins *et al.*, 1986; Signor *et al.*, 1999a; Qin *et al.*, 2001). Typical of retrograde defects, the cilia show a bulb like structure at the distal tip with extensive accumulation of IFT proteins along the axoneme. These data suggest that in *xbx-1* mutants, IFT particles enter the cilium axoneme where they are transported in anterograde direction but then fail to return to the transition zones.

To determine at which step XBX-1 function is required during ciliogenesis, we analyzed how mutations in IFT complex A or B proteins affect the localization of XBX-1::YFP in sensory cilia. In a recent study, we demonstrated that mutations in one complex B protein could differentially affect the localization of other complex B proteins thought to be within the same complex (Haycraft *et al.*, 2003). These data suggest that particle assembly at the transition zone occurs in an ordered process determined by specific protein interactions within the complex. Thus, by placing fluorescence-tagged IFT proteins in the context of different IFT mutants (complex A or B), it may be possible to dissect the hierarchy with which the proteins function in IFT particle assembly and how the A and B complexes interact with each other and the motor proteins. Herein, we observed that none of the complex B mutants analyzed disrupted the ability of XBX-1 to concentrate at the base of the cilia, suggesting that XBX-1 localization and assembly into the particle is independent of the complex B proteins tested. Similarly, our analysis of XBX-1 in complex A mutants revealed that XBX-1::YFP effectively enters the axoneme and is transported to the distal tip of the cilia. Thus, complex A protein function is not required for XBX-1 anterograde IFT movement. Additionally, there was no significant accumulation of XBX-1::YFP in the swollen axonemes of the complex A mutants, unlike that

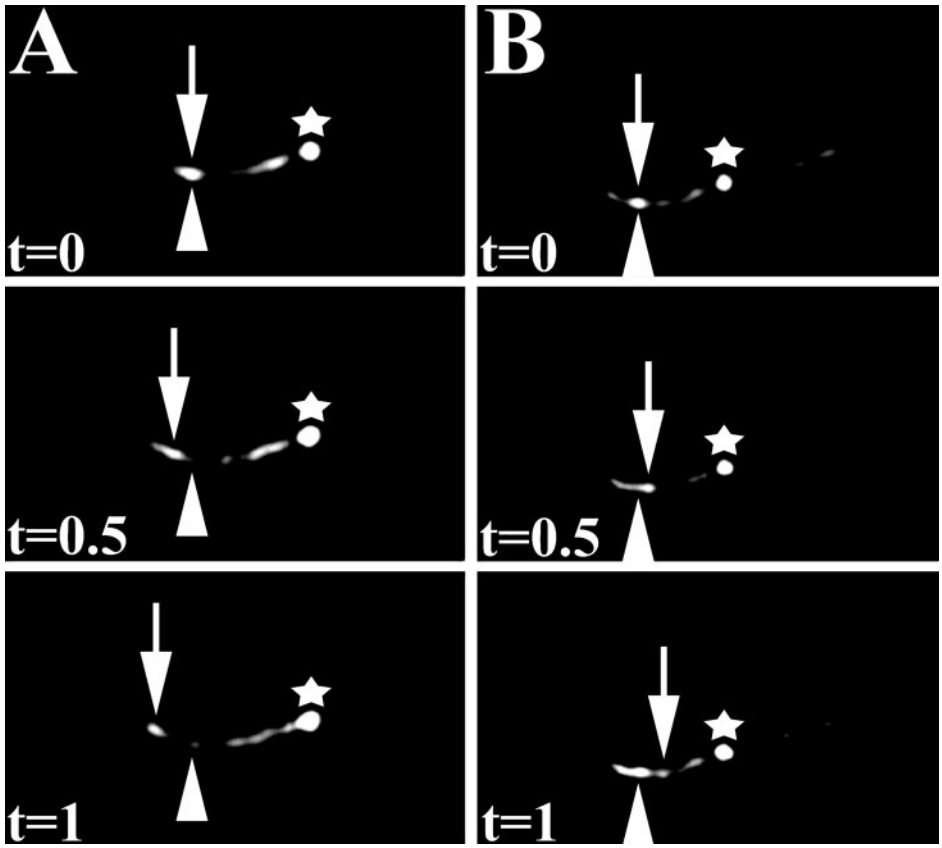

Figure 7. Movement of XBX-1::YFP along the cilia axonemes on one pair of phasmid neurons of a *che-11* complex A mutant. Using time-lapse fluorescence image analysis, XBX-1::YFP movement was observed in the (A) anterograde direction along the stunted cilia axoneme of the *che-11* mutants. In contrast to other IFT proteins, XBX-1::YFP transport was also detected in the (B) retrograde direction. This continued retrograde trafficking of XBX-1 in *che-11* mutants is consistent with the failure of XBX-1 to accumulate in the cilia axoneme. Images were captured at a rate of two frames per second. The distal tips of the phasmid cilia are directed toward the left. The transition zone is marked (*). The arrowhead indicates the initial IFT particle at time zero ($t = 0$). The arrows indicate the same particle at the subsequent times indicated ($t = 0.5$ s, and $t = 1$ s). Three frames representative of the movement seen in Movie 2 are shown for each direction.

observed with the complex B proteins. This is surprising considering the proposed retrograde transport role for complex A proteins. Because XBX-1::YFP fails to accumulate in the cilia of the complex A mutants, we speculated that XBX-1 retrograde transport was not disrupted by the loss of complex A. To test this possibility, we used time-lapse image analysis of XBX-1::YFP in two complex A mutant backgrounds. In contrast to what was seen for other IFT proteins analyzed, XBX-1::YFP retrograde transport was still detected in both complex A mutants. Furthermore, when XBX-1::YFP was analyzed in the *che-3* dynein mutant, XBX-1 retrograde transport was abolished. Collectively, these data suggest that XBX-1 function is required for retrograde IFT in parallel with CHE-3. Moreover, it suggests that XBX-1 activity is required subsequent to proteins in complex A, because the complex A proteins accumulate in *xbx-1* mutants but XBX-1 does not accumulate in the complex A mutants. These data raise the possibility that XBX-1 functions to connect the IFT particle and CHE-3 motor. This possibility is further supported by biochemical evidence in other species showing that the orthologs of XBX-1 both copurify and coimmunoprecipitate with the IFT dynein complex (Grissom *et al.*, 2002; Perrone *et al.*, 2003). Further biochemical and genetic analyses of XBX-1 will be required to confirm whether XBX-1 directly associates with a protein in the IFT particle and/or the CHE-3 dynein motor.

In contrast to the localization of XBX-1 in *che-3(e1124)* mutants reported here, in the *Chlamydomonas cDhc1b* mutants the LIC (the XBX-1 ortholog) is not detected in the stunted flagella (Perrone *et al.*, 2003). However, the complex A and B proteins do accumulate similarly to that seen in the cilia of *che-3* mutant worms (Pazour *et al.*, 1999; Porter *et al.*, 1999). These apparently conflicting effects may be explained by the differences in the dynein mutations. The *che-3(e1124)* strain used in this study has a nonsense mutation located in the middle of CHE-3 and truncates the proteins before the motor domain (Wicks *et al.*, 2000). Although the *che-3* mutation may be a hypomorphic allele, the *Chlamydomonas cDhc1b* (*che-3* ortholog) mutation analyzed by Perrone *et al.* (2003) is a deletion and presumably produces no protein. Because the interaction between the dynein heavy chain and its LIC is thought to occur through the N-terminal region of the dynein (Tynan *et al.*, 2000a), it is likely that XBX-1 and the mutant form of CHE-3 used in our analysis still associate and are transported into the axoneme, where it would then accumulate because of loss of the retrograde motor activity. However, in the *Chlamydomonas cDhc1b* mutants, the putative LIC binding site is lost, thus preventing LIC's entry into the cilium and subsequent movement along the axoneme. Furthermore, these data suggest that because the A and B complexes accumulate in both dynein mutants, their entry into the cilia does not appear to be dependent on the function of the dynein heavy chain/LIC complex.

Dyneins are high-molecular-weight, multisubunit complexes that play diverse roles in the cell (reviewed in Porter and Johnson, 1989; Holzbaur and Vallee, 1994; Hirokawa, 1998). Two classes of dyneins have been identified, including the extensive family of axonemal dyneins required for

cilia and flagella beating and the cytoplasmic dyneins that play a role in intracellular vesicle transport, organelle movement, mitotic spindle assembly, chromosomal segregation, axonal transport, and retrograde movement in IFT (Mitchell, 1994; Porter, 1996; Vaisberg *et al.*, 1996; Hirokawa, 1998; Pazour *et al.*, 1999; Porter *et al.*, 1999; Signor *et al.*, 1999a; Goldstein, 2001). Diversification of dynein function appears to be regulated by the accessory proteins associated with the dynein heavy chains that provide motive force driving movement along the microtubules (Karcher *et al.*, 2002). As discussed above, our data support a role for XBX-1 as an accessory protein to the CHE-3 IFT dynein. This prediction is further corroborated by the recent analysis of orthologs of XBX-1 in both the mouse (D2LIC) and in *Chlamydomonas* (Perrone *et al.*, 2003). In its initial characterization, the mammalian D2LIC was identified as a DLIC that associates with the dynein heavy chain DHC2 (Grissom *et al.*, 2002). Interestingly, DHC2 is the ortholog of the worm CHE-3 and *Chlamydomonas* DHC1b IFT dynein. In mammalian systems, D2LIC and DHC2 were found to localize to the Golgi apparatus and centrosomes of nonpolarized cells where they were thought to be involved in intracellular trafficking and Golgi organization (Grissom *et al.*, 2002). Although the initial report on D2LIC demonstrated no role in ciliogenesis (Grissom *et al.*, 2002), data provided by Perrone *et al.* (2003) do show localization of D2LIC and DHC2 in the cilium of polarized epithelia in vivo and in vitro in MDCK cells. We believe that the different results with regard to D2LIC/XBX-1 protein localization are a direct result of the respective cell types analyzed and the conditions in which these experiments were conducted. The study performed by Grissom *et al.* (2002) was done in COS-7 cells under relatively nonpolarized conditions where cilia are not likely to be present. Furthermore, their expression analysis of D2LIC in various mammalian organs at the level of Western blot shows a good correlation between expression levels and the extent of ciliated cells present in the respective organ. The highest levels of expression were seen in the testis, lung, brain, and kidney, with little expression seen in the heart, liver, and spleen (Grissom *et al.*, 2002). These data parallel the expression profiles seen for polaris, which is known to be a cilia protein in the mouse (Taulman *et al.*, 2001).

In contrast to what was suggested for mammalian D2LIC, we do not believe that either XBX-1 or CHE-3 has a significant role in Golgi organization in *C. elegans.* This is supported by several lines of evidence. First *xbx-1* expression is restricted to a small number of cells, all of which are ciliated. Second, the protein is prominently localized to cilia and third, mutations in *xbx-1* and *che-3* result in cilia specific defects (Perkins *et al.*, 1986; Signor *et al.*, 1999a; Wicks *et al.*, 2000). Although we cannot unequivocally exclude a role for XBX-1 in Golgi, we would predict that disruption of this organelle would have a more profound effect than simply the loss of cilia. An additional possibility is that these proteins have acquired multiple functions in mammals both in the Golgi as seen in COS-7 cells (Grissom *et al.*, 2002) and in cilia as shown in Perrone *et al.* (2003), while retaining a single function in IFT in *C. elegans*. Finally, recent work has shown DHC2/dynein 2 and D2LIC/LIC3 both localize to connecting cilia of photoreceptor cells and primary cilia of cultured kidney epithelial cells (Mikami *et al.*, 2002). Furthermore, no colocalization of either DHC2/dynein 2 or D2LIC/LIC3 with the Golgi was seen (Mikami *et al.*, 2002). This work also notes that although XBX-1 (F02D8.3 protein) shares homology with D2LIC/LIC3, XBX-1 does not contain the same P-loop motif, suggesting that it may have distinct functions in mammals (Mikami *et al.*, 2002).

Cilia assembly is a highly coordinated process in which as many as 200 distinct proteins need to be transported from their site of synthesis in the cytoplasm to their site of function in the axoneme. Proper localization and function of these proteins appear to be regulated by balancing the activity of the IFT kinesin and dynein (Cole *et al.*, 1998; Pazour *et al.*, 1999; Signor *et al.*, 1999a). Thus, to understand how the IFT particle is transported and how cargo specificity is determined will require more detailed analysis of the kinesin and dynein accessory proteins, such as XBX-1. Disruption of this process, as seen in mice with mutations in the *Tg737* gene (complex B), demonstrates the importance of elucidating the mechanism of IFT and cilia function as these mice exhibit major pathologies such as random left-right axis specification, skeletal pattering defects, cystic kidney disease, biliary and bile ductule hyperplasia, hydrocephalus, pancreatic acinar and ductule abnormalities, retinal degeneration, and sterility (Moyer *et al.*, 1994; Murcia *et al.*, 2000; Pazour *et al.*, 2000, 2002; Taulman *et al.*, 2001; Yoder *et al.*, 2002).

ACKNOWLEDGMENTS

We gratefully acknowledge Drs. S. Nozell and M. Porter for critical reading of this manuscript. We thank Drs. A. Coulson and A. Fire for the gifts of *C. elegans* clones and expression vectors and A. Tousson and S. Williams of the UAB Imaging Facility for assistance in fluorescence microscopy. We thank Dr. T. Hays and S. Mische for generous use of the Ultra*VIEW* LCI and assistance with time-lapse imaging. We thank Thomas Bürglin for transiently providing laboratory space. We thank Dr. M. Barr for the CHE-11::GFP transgenic strain used for localization studies and Kerry Bubb for help with computer programming and algorithm design. The *C. elegans* Genome Sequencing Consortium provided sequence information and the *Caenorhabditis* Genetics Center, which is funded by the National Institutes of Health, provided some of the *C. elegans* strains used in this study. We thank the *C. elegans* Knockout Consortium for providing the *xbx-1(ok279)* deletion mutant. This work was supported in part by a Public Health Service grant to J.H.T. (R01 GM48700), by a grant to P.S. from the Swedish Foundation for Strategic Research (SSF) in Stockholm, Sweden, and by Grant RO1-DK-62758 to B.K.Y. from the National Institute of Diabetes and Digestive and Kidney Diseases, and the March of Dimes Research Grant FY01-105.

REFERENCES

Altschul, S.F., Madden, T.L., Schaffer, A.A., Zhang, J., Zhang, Z., Miller, W., and Lipman, D.J. (1997). Gapped BLAST and PSI-BLAST: a new generation of protein database search programs. Nucleic Acids Res. *25*, 3389–3402.

Anderson, P. (1995). Mutagenesis. Methods Cell Biol. *48*, 31–58.

Brenner, S. (1974). The genetics of *Caenorhabditis elegans*. Genetics *77*, 71–94.

Cole, D.G., Diener, D.R., Himelblau, A.L., Beech, P.L., Fuster, J.C., and Rosenbaum, J.L. (1998). Chlamydomonas kinesin-II-dependent intraflagellar transport (IFT): IFT particles contain proteins required for ciliary assembly in *Caenorhabditis elegans* sensory neurons. J. Cell Biol. *141*, 993–1008.

Collet, J., Spike, C.A., Lundquist, E.A., Shaw, J.E., and Herman, R.K. (1998). Analysis of osm-6, a gene that affects sensory cilium structure and sensory neuron function in *Caenorhabditis elegans*. Genetics *148*, 187–200.

Consortium, C.e.S. (1998). Genome sequence of the nematode *C. elegans*: a platform for investigating biology. Science *282*, 2012–2018.

Culotti, J.G., and Russell, R.L. (1978). Osmotic avoidance defective mutants of the nematode *Caenorhabditis elegans*. Genetics *90*, 243–256.

Emery, P., Strubin, M., Hofmann, K., Bucher, P., Mach, B., and Reith, W. (1996). A consensus motif in the RFX DNA binding domain and binding domain mutants with altered specificity. Mol. Cell. Biol. *16*, 4486–4494.

Fujiwara, M., Ishihara, T., and Katsura, I. (1999). A novel WD40 protein, CHE-2, acts cell-autonomously in the formation of *C. elegans* sensory cilia. Development *126*, 4839–4848.

Gibbons, I.R. (1995). Dynein family of motor proteins: present status and future questions. Cell Motil. Cytoskel. *32*, 136–144.

Goldstein, L.S. (2001). Kinesin molecular motors: transport pathways, receptors, and human disease. Proc. Natl. Acad. Sci. USA *98*, 6999–7003.

Grissom, P.M., Vaisberg, E.A., and McIntosh, J.R. (2002). Identification of a novel light intermediate chain (D2LIC) for mammalian cytoplasmic dynein 2. Mol. Biol. Cell *13*, 817–829.

Haycraft, C.J., Schafer, J.C., Zhang, Q., Taulman, P.D., and Yoder, B.K. (2003). Identification of CHE-13, a novel intraflagellar transport protein required for cilia formation. Exp. Cell Res. *284*, 249–261.

Haycraft, C.J., Swoboda, P., Taulman, P.D., Thomas, J.H., and Yoder, B.K. (2001). The *C. elegans* homolog of the murine cystic kidney disease gene Tg737 functions in a ciliogenic pathway and is disrupted in osm-5 mutant worms. Development *128*, 1493–1505.

Hirokawa, N. (1998). Kinesin and dynein superfamily proteins and the mechanism of organelle transport. Science *279*, 519–526.

Holzbaur, E.L., and Vallee, R.B. (1994). DYNEINS: molecular structure and cellular function. Annu. Rev. Cell Biol. *10*, 339–372.

Huang, L.S., Tzou, P., and Sternberg, P.W. (1994). The lin-15 locus encodes two negative regulators of *Caenorhabditis elegans* vulval development. Mol. Biol. Cell *5*, 395–411.

Iomini, C., Babaev-Khaimov, V., Sassaroli, M., and Piperno, G. (2001). Protein particles in Chlamydomonas flagella undergo a transport cycle consisting of four phases. J. Cell Biol. *153*, 13–24.

Karcher, R.L., Deacon, S.W., and Gelfand, V.I. (2002). Motor-cargo interactions: the key to transport specificity. Trends Cell Biol. *12*, 21–27.

Kozminski, K.G., Johnson, K.A., Forscher, P., and Rosenbaum, J.L. (1993). A motility in the eukaryotic flagellum unrelated to flagellar beating. Proc. Natl. Acad. Sci. USA *90*, 5519–5523.

Liu, K.S., and Sternberg, P.W. (1995). Sensory regulation of male mating behavior in *Caenorhabditis elegans*. Neuron *14*, 79–89.

Malone, E.A., and Thomas, J.H. (1994). A screen for nonconditional dauer-constitutive mutations in *Caenorhabditis elegans*. Genetics *136*, 879–886.

Mello, C.C., Kramer, J.M., Stinchcomb, D., and Ambros, V. (1991). Efficient gene transfer in C. elegans: extrachromosomal maintenance and integration of transforming sequences. EMBO J. *10*, 3959–3970.

Mikami, A., Tynan, S., Hama, T., Luby-Phelps, K., Saito, T., Crandall, J., Besharse, J., and Vallee, R. (2002). Molecular structure of cytoplasmic dynein 2 and its distribution in neuronal and ciliated cells. J. Cell Sci. *115*, 4801–4808.

Mitchell, D.R. (1994). Cell and molecular biology of flagellar dyneins. Int. Rev. Cytol. *155*, 141–180.

Moyer, J.H. *et al.* (1994). Candidate gene associated with a mutation causing recessive polycystic kidney disease in mice. Science *264*, 1329–1333.

Murcia, N.S., Richards, W.G., Yoder, B.K., Mucenski, M.L., Dunlap, J.R., and Woychik, R.P. (2000). The Oak Ridge Polycystic Kidney (orpk) disease gene is required for left-right axis determination. Development *127*, 2347–2355.

Nonet, M.L., Saifee, O., Zhao, H., Rand, J.B., and Wei, L. (1998). Synaptic transmission deficits in *Caenorhabditis elegans* synaptobrevin mutants. J. Neurosci. *18*, 70–80.

Orozco, J.T., Wedaman, K.P., Signor, D., Brown, H., Rose, L., and Scholey, J.M. (1999). Movement of motor and cargo along cilia. Nature *398*, 674.

Pazour, G.J., Baker, S.A., Deane, J.A., Cole, D.G., Dickert, B.L., Rosenbaum, J.L., Witman, G.B., and Besharse, J.C. (2002). The intraflagellar transport protein, IFT88, is essential for vertebrate photoreceptor assembly and maintenance. J. Cell Biol. *157*, 103–113.

Pazour, G.J., Dickert, B.L., Vucica, Y., Seeley, E.S., Rosenbaum, J.L., Witman, G.B., and Cole, D.G. (2000). Chlamydomonas IFT88 and its mouse homologue, polycystic kidney disease gene tg737, are required for assembly of cilia and flagella. J. Cell Biol. *151*, 709–718.

Pazour, G.J., Dickert, B.L., and Witman, G.B. (1999). The DHC1b (DHC2) isoform of cytoplasmic dynein is required for flagellar assembly. J. Cell Biol. *144*, 473–481.

Perkins, L.A., Hedgecock, E.M., Thomson, J.N., and Culotti, J.G. (1986). Mutant sensory cilia in the nematode *Caenorhabditis elegans*. Dev. Biol. *117*, 456–487.

Perrone, C.A., Tritschler, D., Taulman, P., Bower, R., Yoder, B.K., and Porter, M.E. (2003). Mol. Biol. Cell *14*, 2041–2056.

Piperno, G., and Mead, K. (1997). Transport of a novel complex in the cytoplasmic matrix of Chlamydomonas flagella. Proc. Natl. Acad. Sci. USA *94*, 4457–4462.

Piperno, G., Siuda, E., Henderson, S., Segil, M., Vaananen, H., and Sassaroli, M. (1998). Distinct mutants of retrograde intraflagellar transport (IFT) share similar morphological and molecular defects. J. Cell Biol. *143*, 1591–1601.

Porter, M.E. (1996). Axonemal dyneins: assembly, organization, and regulation. Curr. Opin. Cell Biol. *8*, 10–17.

Porter, M.E., Bower, R., Knott, J.A., Byrd, P., and Dentler, W. (1999). Cytoplasmic dynein heavy chain 1b is required for flagellar assembly in Chlamydomonas. Mol. Biol. Cell *10*, 693–712.

Porter, M.E., and Johnson, K.A. (1989). Dynein structure and function. Annu. Rev. Cell Biol. *5*, 119–151.

Qin, H.M., Rosenbaum, J.L., and Barr, M.M. (2001). An autosomal recessive polycystic kidney disease gene homolog is involved in intraflagellar transport in C-elegans ciliated sensory neurons. Curr. Biol. *11*, 457–461.

Rosenbaum, J. (2002). Intraflagellar transport. Curr. Biol. *12*, R125.

Sambrook, J., Fritsch, E.F., and Maniatis, T. (1989). Molecular Cloning: A Laboratory Manual. Cold Spring Harbor, NY: Cold Spring Harbor Laboratory.

Signor, D., Wedaman, K.P., Orozco, J.T., Dwyer, N.D., Bargmann, C.I., Rose, L.S., and Scholey, J.M. (1999a). Role of a class DHC1b dynein in retrograde transport of IFT motors and IFT raft particles along cilia, but not dendrites, in chemosensory neurons of living *Caenorhabditis elegans*. J. Cell Biol. *147*, 519–530.

Signor, D., Wedaman, K.P., Rose, L.S., and Scholey, J.M. (1999b). Two heteromeric kinesin complexes in chemosensory neurons and sensory cilia of *Caenorhabditis elegans*. Mol. Biol. Cell *10*, 345–360.

Starich, T.A., Herman, R.K., Kari, C.K., Yeh, W.H., Schackwitz, W.S., Schuyler, M.W., Collet, J., Thomas, J.H., and Riddle, D.L. (1995). Mutations affecting the chemosensory neurons of *Caenorhabditis elegans*. Genetics *139*, 171–188.

Stein, L., Sternberg, P., Durbin, R., Thierry-Mieg, J., and Spieth, J. (2001). WormBase: network access to the genome and biology of *Caenorhabditis elegans*. Nucleic Acids Res. *29*, 82–86.

Swoboda, P., Adler, H.T., and Thomas, J.H. (2000). The RFX-type transcription factor DAF-19 regulates sensory neuron cilium formation in C. elegans. Mol. Cell *5*, 411–421.

Taulman, P.D., Haycraft, C.J., Balkovetz, D.F., and Yoder, B.K. (2001). Polaris, a protein involved in left-right axis patterning, localizes to basal bodies and cilia. Mol. Biol. Cell *12*, 589–599.

Tynan, S.H., Gee, M.A., and Vallee, R.B. (2000a). Distinct but overlapping sites within the cytoplasmic dynein heavy chain for dimerization and for intermediate chain and light intermediate chain binding. J. Biol. Chem. *275*, 32769–32774.

Tynan, S.H., Purohit, A., Doxsey, S.J., and Vallee, R.B. (2000b). Light intermediate chain 1 defines a functional subfraction of cytoplasmic dynein which binds to pericentrin. J. Biol. Chem. *275*, 32763–32768.

Vaisberg, E.A., Grissom, P.M., and McIntosh, J.R. (1996). Mammalian cells express three distinct dynein heavy chains that are localized to different cytoplasmic organelles. J. Cell Biol. *133*, 831–842.

Wicks, S.R., de Vries, C.J., van Luenen, H.G., and Plasterk, R.H. (2000). CHE-3, a cytosolic dynein heavy chain, is required for sensory cilia structure and function in *Caenorhabditis elegans*. Dev. Biol. *221*, 295–307.

Yoder, B.K., Tousson, A., Millican, L., Wu, J.H., Bugg, C.E., Jr., Schafer, J.A., and Balkovetz, D.F. (2002). Polaris, a protein disrupted in orpk mutant mice, is required for assembly of renal cilium. Am. J. Physiol. Renal Fluid Electrolyte Physiol. *282*, F541–F552.